Combustion and Flame 220 (2020) 288–297

Contents lists available at ScienceDirect

Combustion and Flame

journal homepage: www.elsevier.com/locate/combustflame

Agglomeration and combustion characteristics of solid composite propellants containing aluminum-based alloys

Wen Ao[a,*], Zhimin Fan[a], Lu Liu[a], Yuxin An[a], Jiaren Ren[a], Mingtao Zhao[a], Peijin Liu[a], Larry K.B. Li[b]

[a] Science and Technology on Combustion, Internal Flow and Thermo-structure Laboratory, Northwestern Polytechnical University, Xi'an, 710072, China
[b] Department of Mechanical and Aerospace Engineering, The Hong Kong University of Science and Technology, Clear Water Bay, Hong Kong

ARTICLE INFO

Article history:
Received 27 April 2020
Revised 28 June 2020
Accepted 1 July 2020

Keywords:
Solid fuel combustion
Aluminized propellants
Alloy combustion
Agglomeration
Solid rocket motor

ABSTRACT

Agglomeration in solid composite propellants is known to exacerbate two-phase flow losses. In this experimental study, we investigate the substitution of aluminum particles with metallic alloys in order to reduce agglomeration in aluminized propellants. We consider five different aluminum-based alloys: Al-Mg, Al-Ni, Al-Si, Al-B, and Al-Zn. Through thermogravimetric-differential scanning calorimetry measurements, we find that all five alloys can increase the initial oxidation temperature relative to a baseline Al propellant, but that only Al-Si and Al-Zn exhibit lower melting temperatures. Laser ignition experiments show that Al-Mg produces the most balanced combination of a short ignition delay time and a short self-sustaining combustion time. High-pressure experiments at 0.5 to 3 MPa show that Al-Si has a markedly higher burning rate than the baseline Al propellant, while Al-Mg and Al-Ni have the lowest pressure exponents. High-speed microscopic surface imaging at 0.5 and 1 MPa shows that Al-Ni produces the largest reduction in agglomeration, with an average agglomerate size some 30% smaller than the baseline value. By contrast, Al-Zn produces the worst agglomeration, with an average agglomerate size around 15% larger than the baseline value. From these findings, we propose a qualitative phenomenological mechanism for agglomeration in metallic-alloy propellants based on a competition among four distinct effects: the metal melting temperature, the adhesive force of the agglomerates, the propellant burning rate, and micro-explosions. We then analyze the agglomeration of the different alloys using the proposed mechanism. As well as providing new experimental data on the agglomeration, ignition and combustion characteristics of solid composite propellants containing aluminum-based alloys, this study reinforces the notion that the agglomeration and combustion performance of aluminized propellants can be optimized through a judicious choice of alloying elements.

1. Introduction

Aluminum is often used as a fuel additive in composite propellants to increase the specific impulse of solid rocket motors (SRMs). Aluminum is preferred because of its high energy density, low cost, and proven safety. However, aluminized fuel particles are prone to agglomeration, resulting in incomplete chemical energy conversion of the propellant as well as increased erosion of the SRM nozzle walls through increased slag deposition. Furthermore, it is well known that large particles require more energy to accelerate than small particles, leaving less energy in the carrier exhaust gases and hence reducing the specific impulse. To reduce such two-phase flow losses, it is important to investigate how aluminum particle agglomeration can be reduced in the high-pressure combusting environment of an SRM.

Currently there are two main strategies for reducing particle agglomeration in aluminized propellants. The first involves tuning the propellant formulation, such as increasing the concentration of ammonium perchlorate (or 'AP', NH_4ClO_4), reducing the metal content, or introducing a burning-rate catalysis [1]. One may also adjust the binder properties so as to tune the combustion and agglomeration characteristics of the propellant [2,3]. The second strategy involves modifying the aluminized particles themselves in such a way as to make them smaller so that they can burn more quickly [4,5]. Over the past decade, this strategy has attracted growing interest, particularly with the adoption of new materials such as nano-Al [6], metallic alloys [7], fluoropolymer coatings [8], and other inclusions [9]. The relatively low active aluminum content in nano-Al particles, however, reduces the specific im-

* Corresponding author
E-mail address: aw@nwpu.edu.cn (W. Ao).

https://doi.org/10.1016/j.combustflame.2020.07.004

pulse, thus limiting the full potential of this technique in practical applications. Modified aluminized particles coated with fluorine-rich polymers are a promising solution, as fluoropolymers can promote the ignition of aluminum through surface exothermic reactions involving the Al_2O_3 shell and fluorine, yielding AlF_3 to reduce metal agglomeration [4,5,10]. However, the low mechanical strength of fluoropolymer coatings presents a significant challenge to deployment. In recent work, we investigated a new functional material to improve the stability of polytetrafluoroethylene (PTFE) coatings [11]. Nevertheless, fuels containing metallic alloys are known to exhibit higher energy densities than those coated with fluoropolymers; for example, the gravimetric calorific value of boron is even higher than that of aluminum. Furthermore, metallic-alloy fuels tend to be more resistant to mechanical failure because they have no coating interface. Therefore, the use of metallic-alloy particles in place of aluminum particles in solid composite propellants could be a viable strategy for reducing particle agglomeration in SRMs.

Previous studies have investigated how the use of metallic alloys – such as Al-Li, Al-Si, Al-Ni and Al-Mg – can reduce agglomeration in propellants. For example, Reese et al. [12] found that the use of 75 wt.% Al-Ni (mass ratio 5:1) led to a marked reduction in the mean agglomerate size, from 235 to 90 μm. They also found that the propellant surface had thinner and more porous flakes, which were smaller than the agglomerates themselves [12]. Valluri et al. [13] explored the use of fuel-rich Al-NiF_2 composites and found that they shortened the ignition delay time relative to baseline Al particles. Terry et al. [14] found that the use of Al-Si enhanced agglomeration owing to greater fluidity on the burning surface. Terry et al. [15] and Hatem et al. [7] investigated the use of Al-Li and Al-Mg particles, respectively, and found that they reduced two-phase flow losses owing to a unique micro-explosion phenomenon that leads to faster metal combustion and smaller particles in the associated plume. Despite significant progress in improving the combustion and agglomeration characteristics of aluminum alloys, the propellant formulations and experimental conditions used in previous studies have been highly variable, making it difficult to develop a unified understanding of the effect of metallic alloys on propellant performance. Such an understanding, however, is needed as a basis for using metallic alloys in solid composite propellants and can guide the exploitation of newly available materials. In addition, Al-Zn [16] and Al-B [17] have been used in solid propellants to improve ignition and combustion, but their agglomeration behavior is still not fully understood. In particular, the micro-agglomeration behavior of different metallic alloys need to be studied in more detail before their potential as a propellant replacement can be further exploited in SRMs.

In this experimental study, we investigate the effects on agglomeration and combustion arising from the replacement of baseline Al particles with five different metallic alloys: Al-Ni, Al-Si, Al-B, Al-Mg and Al-Zn. We benchmark these five alloys against the baseline Al particles through an analysis of their morphology and composition, thermal reactivity, ignition delay times, self-sustaining combustion times, burning rates, ideal specific impulse, and agglomerate sizes. We then conclude by presenting a qualitative phenomenological mechanism for the agglomeration of metallic-alloy propellants.

2. Experimental methodology

This study uses a baseline aluminum powder, with a nominal particle diameter of 40 μm, along with five aluminum-alloy powders containing 10 wt% Si, Zn, Mg, B, and Ni inclusions. These powders were supplied by the Hubei Institute of Aerospace Chemo-Technology. The alloy powders were prepared by cold spraying, in which raw metal ingots were dissolved, mixed and then atomized. The final powders were collected after natural cooling. Solid composite propellants were prepared with the six aforementioned fuel additives: a baseline Al powder and five Al-alloy powders. All six formulations contain 17 wt.% metallic fuel, 60 wt.% AP with a particle diameter of 100 μm, 10 wt.% RDX with a particle diameter of 85 μm $(CH_2NNO_2)_3$, and 13 wt.% hydroxyl terminated polybutadiene (HTPB) as a binder. These specific components were chosen because they constitute the typical formulations found in the rocket industry, thus rendering our results applicable to practical systems.

Thermogravimetric-differential scanning calorimetry (TG-DSC) measurements were carried out on a thermal analysis system in which samples were heated from 30 to 1555 °C at a rate of 10 °C min^{-1}. Oxygen was used as the reacting gas, at a flow rate of 40 mL min^{-1}. Around 1 mg of sample material was used in each test.

A laser ignition system was used to quantify the ignition and combustion characteristics of the propellant samples. The full details of this system can be found in Ref. [11]. The laser was operated at a power setting of 150 W, with a pulse duration of 2 s. Around 50 mg of sample material was used in each test. Flame formation and evolution were recorded with a high-speed camera at a frame rate of 2700 Hz. AP oxidizer was mechanically mixed with the sample to aid ignition.

Figure 1 shows the high-pressure combustion diagnostics system used for propellant testing. This system is identical to that used in our previous studies [18,19], so only a brief overview is given here. The propellant samples were prepared into 20 × 3 × 1 mm strands and covered with insulation material. A spark ignitor made of inflammable material was placed at the top of the propellant. Combustion experiments were conducted in a nitrogen atmosphere at room temperature. An initial high-pressure environment was set up by filling the combustion chamber with nitrogen gas supplied from storage tanks. The combustion and agglomeration characteristics were examined at 8400 frames per second via a high-speed camera (Phantom M340, USA) viewing through a long-distance microscope. The exposure time of each frame was set to 30−45 μs depending on the chamber pressure and the flame intensity of the propellant samples. Because propellants burn at high pressures in SRMs, tests were conducted at four different elevated pressures: 0.5, 1.0, 2.0, and 3.0 MPa. Each propellant was tested three times, and the results were averaged to aid repeatability. The burning rate was measured via pressure signals, with a statistical uncertainty of ±0.2 mm/s. The total burning time t_b of a propellant sample can be determined via the pressure signal in the combustion chamber. The length L of the propellant was measured before ignition, implying that the burning rate r_b can be calculated as L/t_b. This method was also adopted in our previous study (see Ref. [20]).

A scanning electron microscope (SEM) was used to capture high-magnification images of the powder samples. The samples were mounted on an aluminum pin with carbon adhesive tape. The phase compositions of the propellant powder and the condensed combustion products were analyzed with an X-ray diffractometer (XRD) manufactured by Malvern Panalytical (Empyrean).

3. Results and discussion

3.1. Particle morphology and composition

First we examine the particle morphology of the six powders using the SEM described in §2. Figure 2 shows consolidated SEM images of the different powders. The particles in all six powders are predominantly spherical, although some are more irregularly shaped than others, with elongated structures appearing sporadi-

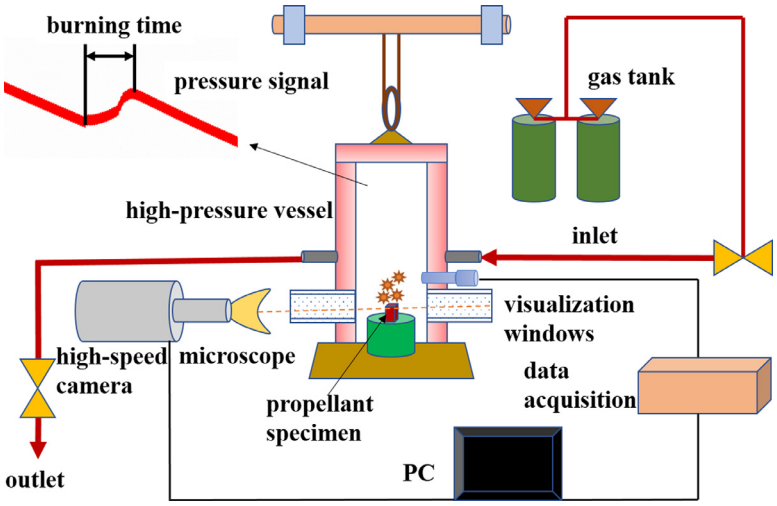

Fig. 1. Schematic of the high-pressure combustion diagnostics system used for propellant testing.

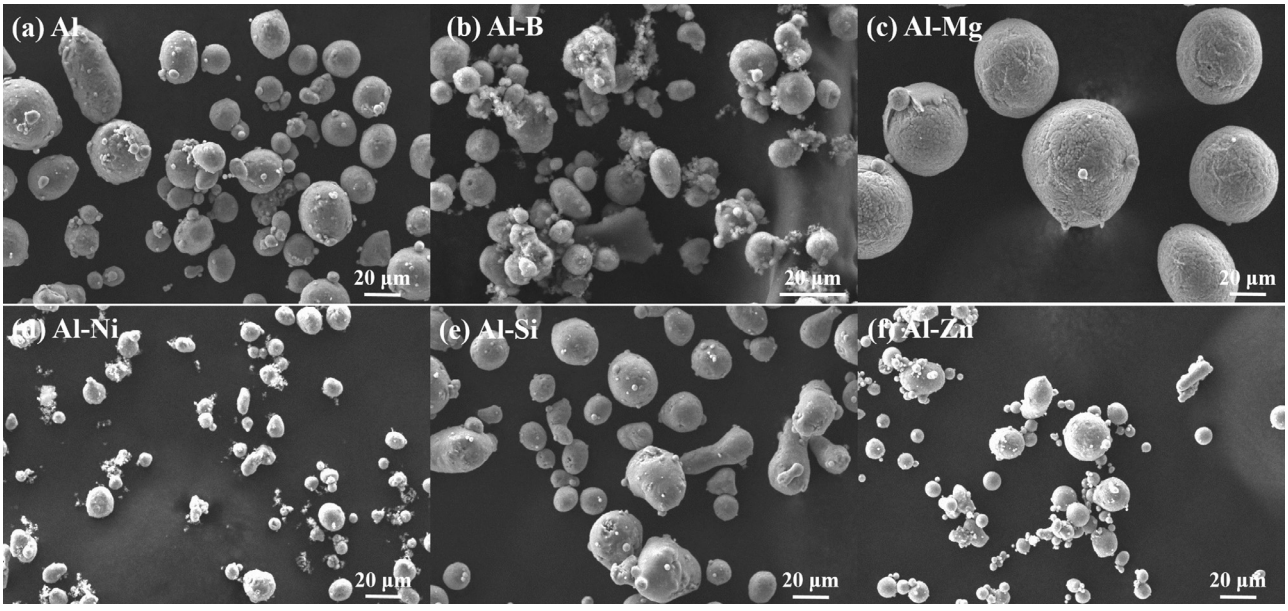

Fig. 2. SEM images of the six powders used in this study: (a) Al, (b) Al-B, (c) Al-Mg (d) Al-Ni, (e) Al-Si, and (f) Al-Zn.

cally. The Al-Mg particles are by far the largest, followed by the Al, Al-Si and Al-B particles, with the Al-Ni and Al-Zn particles coming in at the smallest.

Figure 3 shows the XRD patterns for all six powders. The XRD pattern for the baseline Al shows only peaks corresponding to aluminum, as expected. The XRD pattern for Al-B also shows only peaks corresponding to aluminum. This is because the raw alloy material used in the Al-B sample is amorphous boron, which has been shown to present no obvious diffraction peaks [21]. The XRD pattern for Al-Mg shows peaks corresponding to Al and the intermetallic phase Mg_2Al_3, indicating species diffusion during the melting, mixing and/or atomization processes. There is, however, no significant intermetallic composition found in the Al-Ni, Al-Si and Al-Zn powders. This may be because Ni, Si and Zn are all less reactive than Mg. The diffraction peaks corresponding to Ni, Si and Zn are much weaker than those of the main Al phase.

3.2. Thermal oxidation reactivity at high temperatures

Figure 4 shows the TG-DTG-DSC curves for all six powders, while Table 1 lists their corresponding oxidation reaction prop-

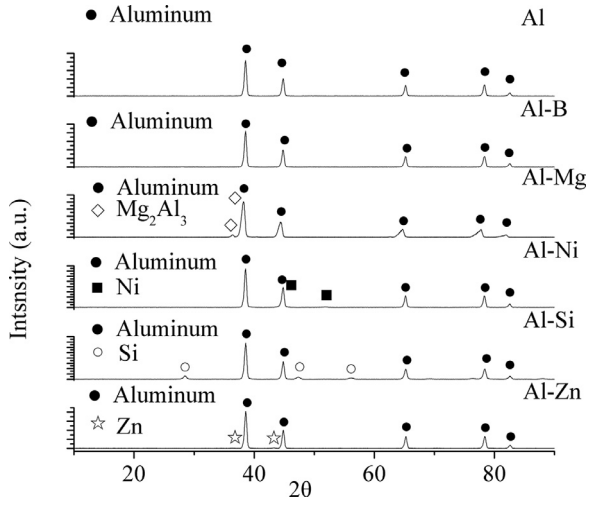

Fig. 3. XRD patterns for the six powders used in this study: a baseline Al powder and five Al-alloy powders.

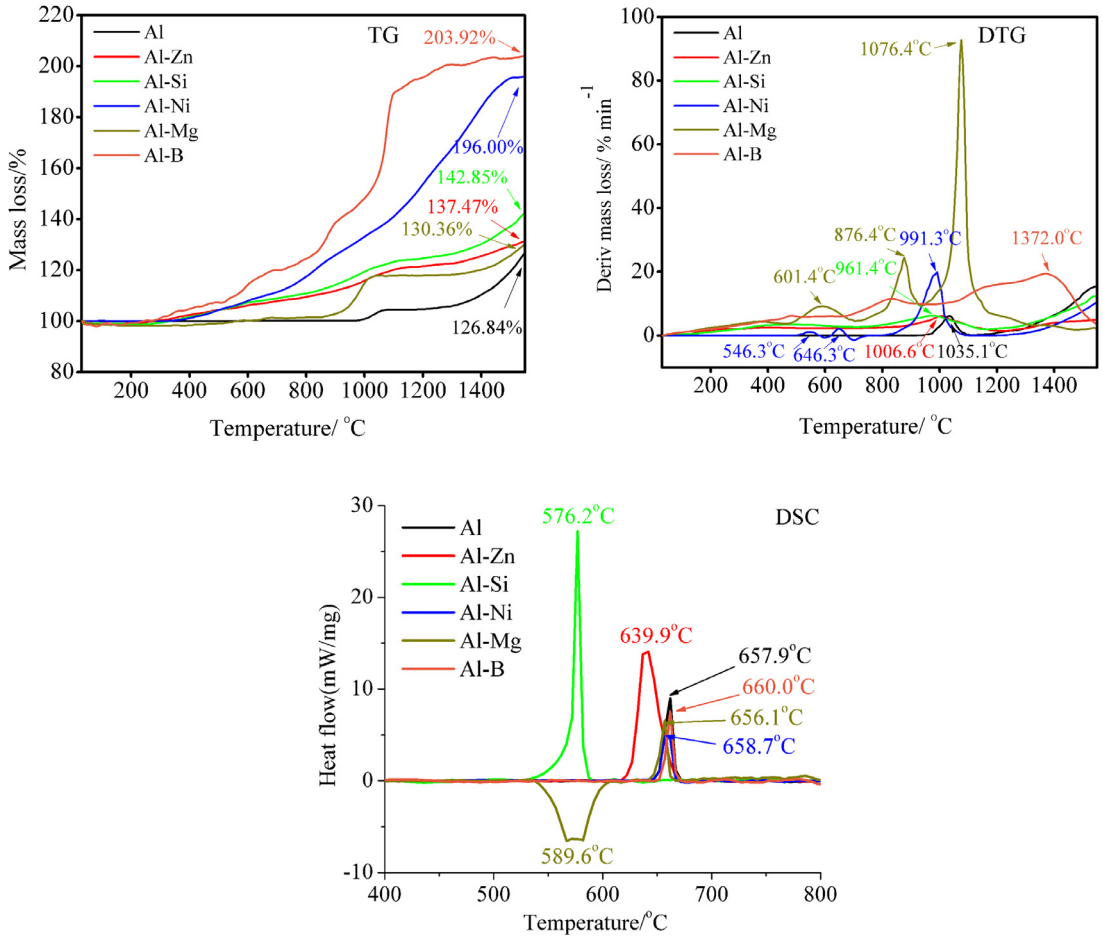

Fig. 4. TG-DTG-DSC curves for the six powders used in this study: a baseline Al powder and five Al-alloy powders. The heating rate is 10°C min^{-1}, from 30 to 1550°C.

Table 1
Oxidation reaction properties of the six powders[a].

Sample	Reaction	TG			DTG		DSC	
		T_i	T_e	Δm	T_{p1}	I_{max}	T_{p2}	Δh
Al	Stage I	965.1	1105.1	4.29	1035.1	6.10	657.9	554
	Stage II	1190.1	NA[b]	22.25	1530.1	15.31	/	/
Al-Zn	Stage I	861.6	1171.6	8.55	1006.6	5.67	639.9	314
	Stage II	1281.6	NA	28.92	1456.6	4.65	/	/
Al-Si	Stage I	306.4	646.4	8.58	476.4	3.12	576.2	829
	Stage II	806.4	1156.4	13.06	961.4	5.74	/	/
	Stage III	1231.4	NA	17.71	1471.4	8.12	/	/
Al-Ni	Stage I	476.3	596.3	4.41	546.3	3.00	658.7	359
	Stage II	606.3	691.3	2.80	646.3	4.02	/	/
	Stage III	826.3	1096.3	20.94	991.3	19.94	/	/
	Stage IV	1201.3	NA	175.06	NA	NA	/	/
Al-Mg	Stage I	511.4	706.4	12.74	601.4	8.12	589.6	−1308
	Stage II	801.4	946.4	18.18	876.4	23.40	656.1	344
	Stage III	951.4	1121.4	48.00	1076.4	91.74	/	/
Al-B	Stage I	327.0	632.0	9.00	482.0	3.90	660.0	337
	Stage II	672.0	937.0	17.99	837.0	9.46	/	/
	Stage III	1037.0	1522.0	59.78	1372.0	17.23	/	/

Note: [a] T_i is the initial temperature at which a mass increase occurs [°C]; T_e is the final temperature of the mass increase [°C]; Δm is the relative mass increase [%]; T_{p1} and T_{p2} are the peak temperatures of the mass increase rate and the heat release, respectively [°C]; I_{max} is the maximum mass increase rate [% min^{-1}]; Δh is the heat release.
[b] NA denotes unfinished reactions up to 1550°C.

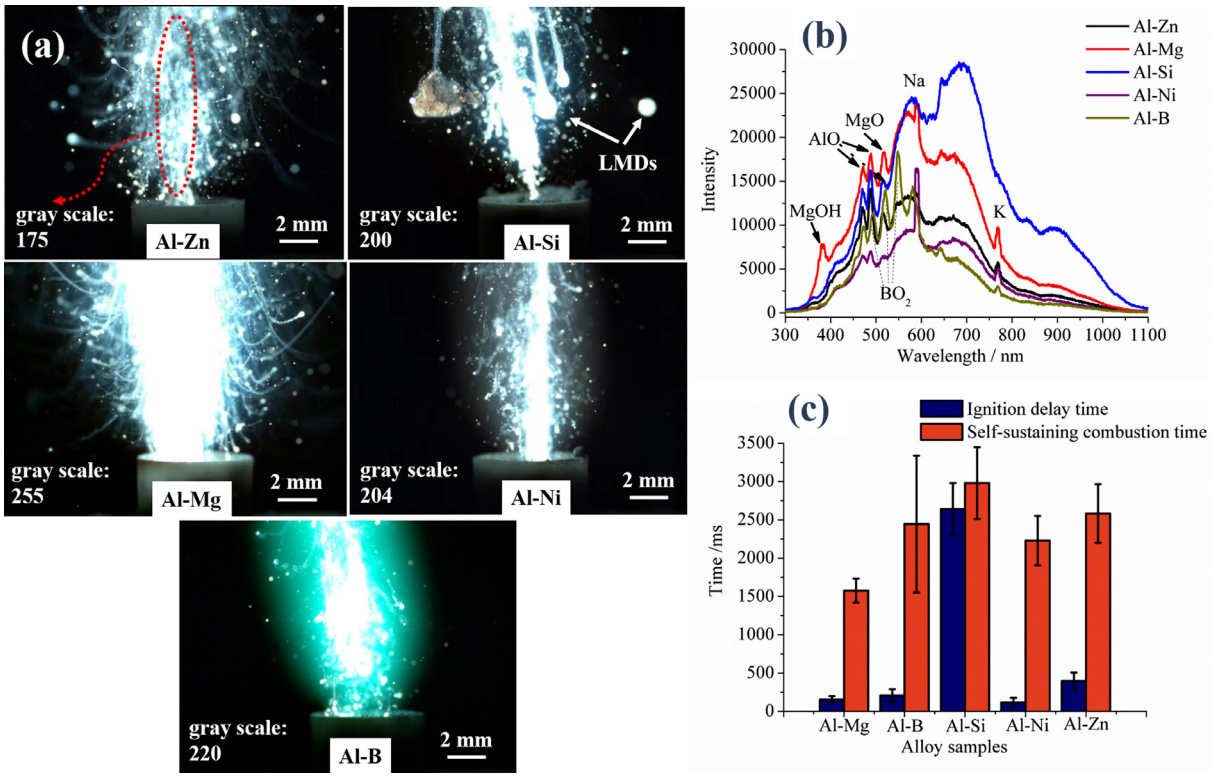

Fig. 5. Ignition and combustion characteristics as measured in laser ignition experiments for five Al-alloy powders: (a) chemiluminescence images of the flame created with different metal-AP powders at atmospheric pressure, (b) maximum spectra at full wave, and (c) ignition delay time and self-sustaining combustion time. In subfigure (a), the term LMD denotes large molten droplets. The error bars in subfigure (c) represent the limits of three replications. (For interpretation of the references to colour in this figure legend, the reader is referred to the web version of this article.)

erties. For the baseline Al powder, the TG curve shows two distinct stages of mass increase, one beginning at 965.1 °C and the other at 1190.1 °C. Here the initial temperature of the Al-O_2 reaction is higher than that reported by Zhou et al. [22] for small Al particles (<10 μm) owing to differences in the specific surface area. At the first stage of mass increase, the oxide transforms from amorphous alumina to crystalline Al_2O_3, possibly α-Al_2O_3 [23]. The newly formed Al_2O_3 covers the aluminum surface, preventing further oxidation. After sufficient heat accumulation, the temperature rises to 1190.1 °C, inducing secondary rapid oxidation. Compared with the baseline Al, Al-Zn exhibits broadly similar trends in its mass variation but a larger total mass increase of 137.47%. This is because the low melting point of Zn (419.5 °C) reduces the melting point of Al-Zn to 639.9 °C, according to the DSC data (the melting point of Al is 657.9 °C). The condensed phase reaction is important to oxidation, so the initial temperature of Al-Zn oxidation is reduced by around 100 °C. However, the rate of mass increase for Al-Zn is reduced owing to the lower reactivity of Zn relative to Al itself. Unlike the two foregoing powders, Al-Si shows evidence of a three-stage reaction, with the initial reaction temperature being as low as 306.4 °C and the total mass increase reaching 142.85%. The corresponding DSC data reveal a lower melting point of 576.2 °C, which is consistent with the measurements of Terry *et al.* [14], who analyzed an Al-Si eutectic alloy with 100 mL/min of oxygen-argon at 20 °C/min. The Al-Ni powder undergoes more elaborate reactions involving four stages of mass increase. Although the melting point of Al-Ni (658.7 °C) is similar to that of Al (657.9 °C), replacing Al with Al-Ni particles still leads to a significant total mass increase of 196% with a lower initial reaction temperature of 476.3 °C. In addition, the maximum rate of mass increase for Al-Ni occurs at around 1000 °C and is nearly twice that of the baseline Al. This suggests that Al-Ni oxidation begins in the condensed phase, effectively raising the subsurface temperature, thus accelerating the reaction rate and efficiency of oxidation. Among the six samples, Al-Mg shows the highest reaction rate: 91.74 at 1076.4 °C. The corresponding DSC data show an exothermic peak at 589.6 °C, which is driven by Mg oxidation, followed by an endothermic reaction associated with the melting of Al at 656.1 °C. The exothermic reaction before the melting of Al is thought to be crucial to the subsequent oxidation of the Al particles, for it plays the role of an activation factor in the oxidation of aluminum. The Al-B sample has the highest total mass increase (203.92%) as well as the hottest peak in mass increase (1372.0 °C). The high-temperature mass increase is likely due to the presence of boron, which causes a large mass increase due to oxidation, even beyond 1200 °C [21]. From these findings, it can be concluded that Al-Si, Al-Ni, Al-Mg and Al-B all promote aluminum oxidation, but only Al-Mg has a positive effect on the reaction rate. Another key observation is that the melting point of Al-Si differs significantly from those of the other samples, which could affect the metal agglomeration behavior on the burning surface of the propellants [5].

3.3. Laser ignition experiments

Laser ignition experiments are performed to examine the ignition and combustion characteristics of the Al and Al-alloy propellants. Figure 5(a) shows chemiluminescence images of the flames created with different metal-AP powders at atmospheric pressure. The flame from the baseline Al sample is not shown because it could not be ignited, even with prolonged laser exposure. This in itself shows that all the metal inclusions tested here can promote Al ignition, just as they can promote Al oxidation, according to the TG-DSC data of Fig. 4. All the flames are blown upwards as a

result of the rapid decomposition of AP, forming a large amount of gaseous products. The emission patterns of the Al-Zn and Al-Si flames appear more discrete than the others, with several large molten droplets clearly visible in the flame core. In particular, a large unburned molten mass can be seen moving upstream (downwards) in the Al-Si flame. The DSC data from Fig. 4 show that the melting points of Al-Si and Al-Zn are the lowest among all six samples tested. This suggests that a low melting point is conducive to sintering and agglomeration of metal particles. By contrast, the metal particles in the Al-Mg, Al-Ni and Al-B flames appear to be smaller and burning in vapor-combustion mode. The Al-Mg flame is the widest, indicating a large area of the burning surface. The Al-B flame is dominated by intense green emission from BO_2, a gas-phase reactant present during boron combustion [24]. To quantify the combustion intensity of the metal particles, we examine the burning surfaces by converting the chemiluminescence images to gray scale and extracting the average pixel count. We then use this as an indicator of the combustion intensity, in accordance with our previous work [11]. Analysis of such images shows that the combustion intensity of the samples decreases in the following order: Al-Mg → Al-B → Al-Ni → Al-Si → Al-Zn. This trend is consistent with the maximum rate of mass increase observed in the oxidation reaction (see Fig. 4) and can be explained by recognizing that metallic fuels with higher reaction rates typically burn more quickly and therefore exhibit higher combustion intensities.

Spectral data collected from the laser ignition experiments are shown in Fig. 5(b) for the five Al-alloy powders; each curve represents the average of three individual test runs. AlO is a known gas-phase intermediate of Al combustion [25]. Here the AlO spectral peaks at 471, 486 and 512 nm are consistent with those found in our recent work [11]. The peaks at 492.9, 518.1, 547.1 and 620.2 nm are attributed to BO_2 emission [26]. The peak at 518 nm arises from gaseous Mg vapor, while that at 385 nm arises from MgOH, which suggests the presence of water vapor from AP decomposition in the combustion environment. Na [27] and K are also detected at 589 and 768 nm, respectively. It can be seen that Al-Si has the strongest overall emission spectrum, which can be attributed to the combustion of large molten droplets. The presence of such droplets may have reduced the receiving distance of the spectral emission signal detected by the spectrometer, resulting in Al-Si having the strongest emission spectrum. According to Fig. 5(c), the ignition delay time increases in the following order: Al-Ni → Al-Mg → Al-B → Al-Zn → Al-Si. This is in stark contrast to the earlier TG results showing that the initial oxidation temperature of Al-Si is the lowest, which implies that the heating rate has a profound effect on metal ignition. Under high heating rates, cracking of the oxide shells occurs as a result of differences in thermal expansion between aluminum and aluminum oxide. Molten metal can leak through cracks and holes in the oxide shell [28]. Moreover, it is well known that small particles can enhance the gas-solid reaction via an increase in the specific surface area. The short ignition delay can be partly attributed to the small size of the Al-Ni particles. Furthermore, the self-sustaining combustion time of Al-Mg is the shortest of all the samples, while its ignition delay time is the second shortest. Overall this shows that Al-Mg exhibits a balanced tradeoff between ignition and combustion performance, while Al-Si performs the worst among all five Al-alloy powders.

3.4. Burning rate and energy performance

Figure 6 shows the burning rates of all six propellants at pressures ranging from 0.5 to 3.0 MPa. It can be seen that, at pressures above 0.5 MPa, replacing baseline Al with Al-Si leads to a marked rise in the burning rate, along with an increase in the pressure exponent – from 0.50 to 0.74. The high fluidity of Al-Si is thought to promote preheating of the condensed phase through chemical reactions involving the decomposition products of AP or HTPB [14], which might explain the increased propellant burning rate. Moreover, Al_2O_3 produced by the ignition enhancement of Si could serve as a catalyst for AP decomposition [10]. Over the entire pressure range tested, the burning rate of the Al-Zn propellant is found to be similar to that of the baseline Al propellant. At pressures above 1 MPa, the Al-B, Al-Mg and Al-Ni propellants have lower burning rates than the baseline Al propellant, with Al-Ni showing a particularly low pressure exponent of 0.29 (vs. 0.50 for baseline Al). The combustion of an AP composite propellant can be divided into three zones: (I) a heat conduction zone in the solid phase, (II) a preparation zone in the gas phase, just above the burning surface, and (III) an exothermic reaction zone. The pressure sensitivity of the heat transfer from zone III to zone II has a strong influence on the pressure exponent. It is therefore conceivable that Ni alters the reaction between the fuel gas produced by the decomposed binder and the AP flamelet, because Ni particles can act on the reaction in the dark zone of a double-based propellant [29]. Chemical equilibrium calculations show that the flame temperature of the Al-B propellant is the lowest of all six propellants, which could explain the low burning rate as arising from reduced thermal feedback. Although boron has a relatively high energy density, there is insufficient oxygen for it to release its full chemical energy. The Ni-Al reaction could modify the structure of the condensed-phase thermal wave, leading to an approximately constant burning rate, as reported by Reese et al. [12]. When the pressure falls below 1 MPa, the burning rate of Al-Mg is actually slightly higher than that of the baseline Al, but drops below it when the pressure rises above 1 MPa. According to our laser ignition experiments (Fig. 5), which were done at atmospheric pressure, Al-Mg shows excellent ignition and combustion performance, with strong heat release on the propellant surface. However, because Mg has a lower vaporization temperature than Al, the endothermic enthalpy of vaporization tends to hinder reactions on the propellant surface [7], thus reducing the burning rate. This indicates that the burning rate of a composite propellant is mainly dependent on the heat release reaction of AP-HTPB on the burning surface, rather than on the thermal feedback of metal combustion in the plume, especially at low pressures [30]. Compared with the baseline Al propellant, Al-Mg has a lower pressure exponent (0.30 vs 0.50). This is similar to magnalium propellants but different from propellants containing Al-Mg alloy (52.6 wt.% Mg) [7]. As our XRD data show (Fig. 3), an intermetallic phase Mg_2Al_3 is present in the Al-Mg alloy, so in this sense it is similar to a magnalium material. Potential differences may be attributed to variations in Mg content and to varia-

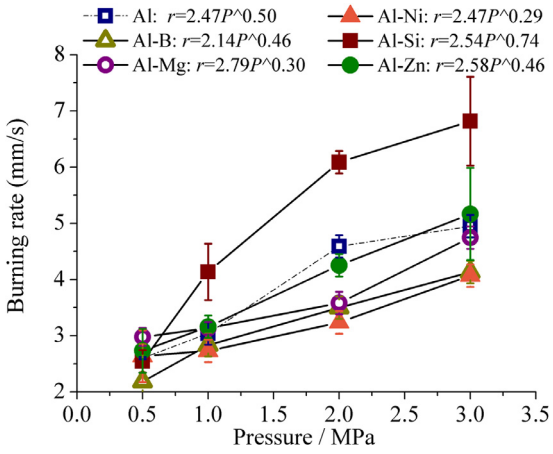

Fig. 6. Experimentally measured burning rates for the Al and Al-alloy propellants. (For interpretation of the references to colour in this figure legend, the reader is referred to the web version of this article.)

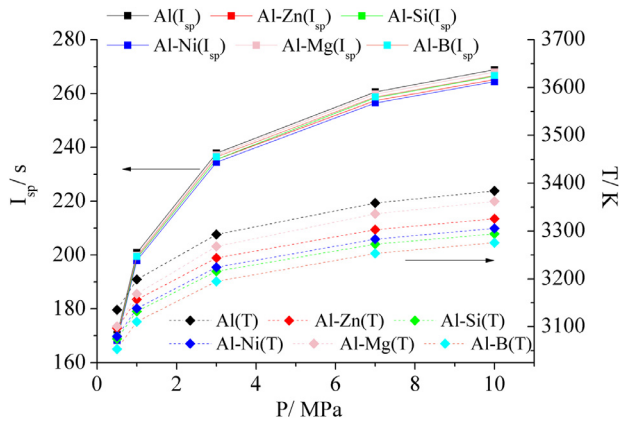

Fig. 7. Ideal specific impulse and adiabatic flame temperature as a function of the chamber pressure (0.5 – 10 MPa, ideal expansion to 0.1 MPa) for the baseline Al propellant and for five Al-alloy propellants.

tions in the particle production process. For example, the powder used in Ref. [7] was produced by mechanical milling, whereas that used here was produced by cold spraying, as discussed in §2.

The specific impulse I_{SP} is a key quantity for evaluating the potential suitability of a new propellant for SRM applications. Therefore, we compute the ideal specific impulse and the adiabatic flame temperature of our propellant formulations using NASA's Chemical Equilibrium with Applications software. The results, presented in Fig. 7, show that, despite differences in their ignition and burning rates, all the Al-alloy propellants tested here give only a slightly lower specific impulse than the baseline Al propellant, which can be explained by the slightly lower adiabatic flame temperatures. At a representative pressure of 7 MPa, Al-Mg gives the highest specific impulse (259.8 s) of the five Al-alloy propellants, while Al-Ni gives the lowest (256.5 s). Nevertheless, it should be noted that even the lowest specific impulse (Al-Ni: 256.5 s) is only 1.6% less than that of the baseline Al propellant (260.6 s). By comparison, previous work [5] has shown that 10 wt.% PTFE can reduce the adiabatic flame temperature, but can increase the specific impulse by 0.7% (from 262.5 to 260.6 s) relative to the baseline propellant. Although fluoropolymers have a lower energy density than most alloys, the loss of specific impulse is reduced compared with Al-Ni. This is because the specific impulse of a propellant is dependent on the energy density, oxygen balance, and interactions between propellant formulations.

3.5. Agglomeration characteristics

Figure 8 shows images of the agglomeration process for the baseline Al particles. The coral structure, agglomerate, and Al droplet with an oxide cap can be readily identified, and are consistent with previous studies [11,18]. In these images, the final agglomerate diameter is around 300 μm, and the total residence time is 16.8 ms. Oxide condensation can also be seen. Typically, an oxide coating covers the particle surface during the ignition process. According to DesJardin et al. [31], this coating can peel back and deposit on the particle itself to form an oxide cap (see Fig. 8c). A convective tail can also be observed emanating from a diffusion flame. This tail is formed from the aluminum oxide transported around the inner droplet by the upward-moving convective flow. Metal agglomeration is known to depend on the fraction of 'pockets' in the propellant formed by coarse AP particles. Figure 8(d) shows an example of secondary agglomeration of the emerging agglomerates, which could be attributed to inter-pocket agglomeration [32].

Next we examine the size of the luminous particles during their ignition and subsequent release from the propellant surface. For each propellant, we identify approximately 200 to 300 agglomerates, and then compute their average particle diameter using size distribution data [11]. It should be noted that the size data for propellant combustion at 2 and 3 MPa were difficult to acquire because many particle images were overexposed, leading to pixel saturation. Therefore, only data for 0.5 and 1 MPa are used, as shown in Fig. 9(a). At a pressure of 0.5 MPa, the nominal agglomerate size of each of the six propellants exceeds 200 μm. Compared with the baseline Al propellant, the Al-Ni propellant produces the smallest particles (210 vs. 226 μm), implying that agglomeration is substantially reduced.

Increasing the ambient pressure from 0.5 to 1 MPa leads to a reduction in particle diameter for all six propellants. It should be noted, however, that increasing the ambient pressure also increases the burning rate, leading to faster detachment of particles from the burning surface [33]. Despite this, the Al-Ni propellant still has the smallest particle size by a significant margin, implying that its agglomeration reduction is the most robust. The use of Al-Ni reduces the mean agglomerate size from 196 to 138 μm at a pressure of 1 MPa. This is consistent with the findings of Ref. [34], in which the use of a nickel coating reduces the agglomerate size from 223 to 138 μm at 1.5 MPa, despite the use of a different binder (isoprene rubber and oil) in the propellant [34]. The use of Al-Mg causes an agglomerate size reduction of 14 μm. As noted by Belal et al. [7], the micro-explosion of Al-Mg particles can lead to particle shattering and enhanced fragmentation, thus reducing the particle size. Evidence of such micro-explosion events is also present in our experiments, as shown in Fig. 9(d). An initial particle suddenly develops a bright glow flame and then disintegrates into two parts owing to a micro-explosion event occurring within 0.2 ms. By contrast, the Al-Zn propellant has the largest agglomerates, with their average diameter around 17% larger than that of the baseline Al propellant at a pressure of 1 MPa. This could be attributed to the low melting point of Al-Zn (639.9 °C), which has the potential to increase the agglomeration of metal particles in the pocket. Thus, an increase in inter-pocket agglomeration would be expected. Like the effect of RDX on agglomeration [19], the introduction of low-melting-point inclusions in the pocket geometry

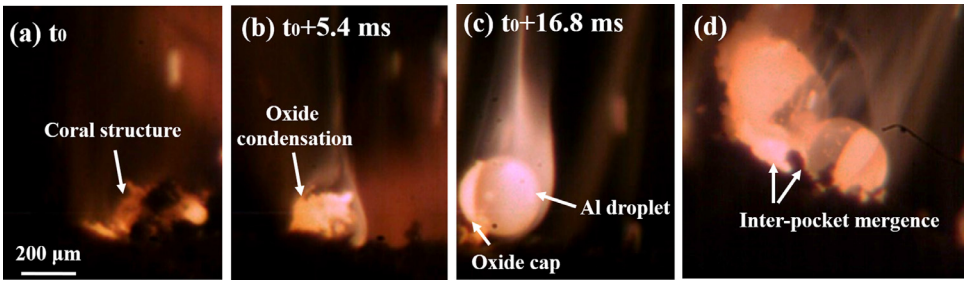

Fig. 8. Typical agglomeration and inter-pocket agglomeration processes on the burning surface of baseline Al particles at a pressure of 0.5 MPa.

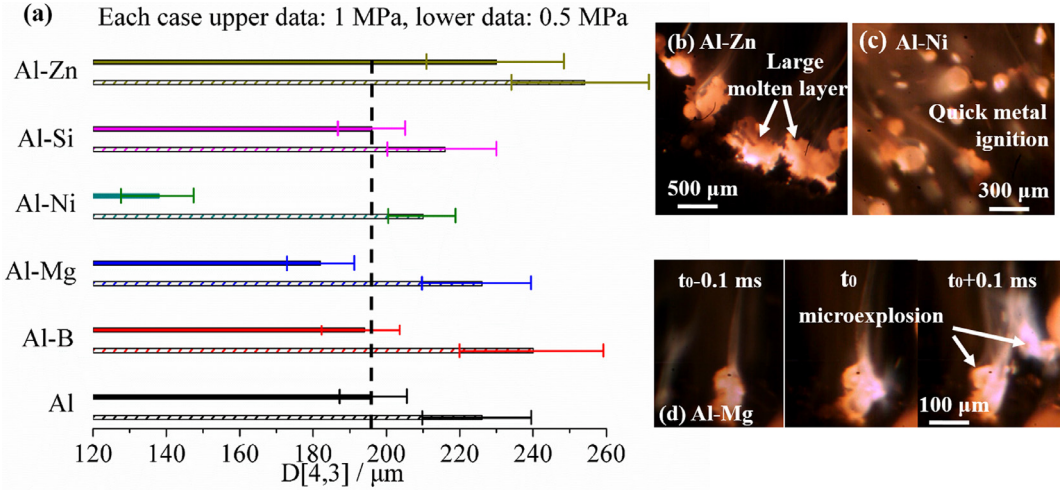

Fig. 9. (a) Mass-averaged diameter of particles near the burning surface of six propellants at two elevated pressures: 0.5 and 1 MPa. Also shown are high-magnification images of the burning surface, with different agglomerate features highlighted: (b) Al-Zn, (c) Al-Ni, and (d) Al-Mg.

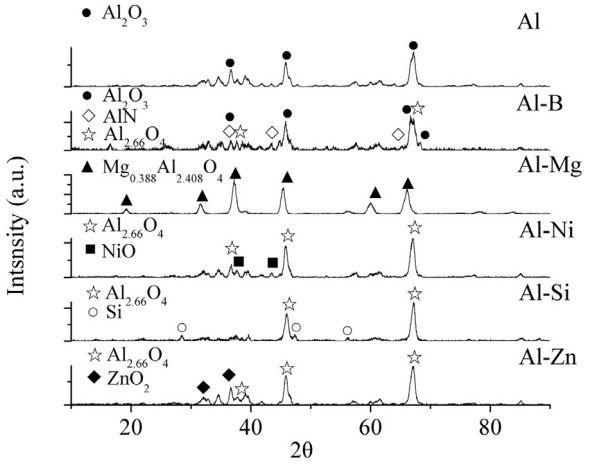

Fig. 10. XRD patterns for the combustion products of the Al and Al-alloy propellants at 3 MPa.

would lead to earlier metal sintering, yielding larger particles. A significant molten layer can be seen on the burning surface of the Al-Zn propellant (Fig. 9b), supporting the aforementioned hypothesis. It should be noted, however, that Al-Si has a melting point (576.2 °C) even lower than Al-Zn, but its agglomerates are roughly the same size as those of the baseline Al propellant. This highlights the important effect that the burning rate has on particle agglomeration: the burning rate of Al-Si is 38% higher than that of Al at a pressure of 1 MPa. Although Terry et al. [14] found that Al-Si-based propellants have larger agglomerates than Al-based propellants, the burning rates of the two were found to be similar. The Al-B propellant has agglomerates similar in size to those of the baseline Al propellant. Although the Al-B propellant has a lower burning rate, we speculate that, for this particular propellant, there is a certain tradeoff against the effect of the burning rate.

Figure 10 shows XRD patterns for the combustion products of the Al and Al-alloy propellants at 3 MPa. It is clear that inclusion of alloys can alter the oxide properties of Al. The condensed combustion product of the baseline Al propellant is primarily Al_2O_3, whereas $Al_{2.66}O_4$ is found in the main products of almost all the alloy propellants tested here. In particular, the products of the Al-Mg propellant includes $Mg_{0.388}Al_{2.408}O_4$. This implies that alloy inclusions significantly affect the crystalline structure of aluminum oxide, further altering the physical and chemical properties of the oxide.

3.6. Agglomeration mechanisms

Existing theoretical models can be classified into four groups: empirical models, physical models (skeleton layer models), pocket models, and packing-based models [35]. Of particular relevance is the skeleton layer (SL) model proposed by Babuk [32], which is well established in the field of propellant agglomeration (see Fig. 11a). The SL is a condensed-phase zone in the upper part of the burning surface, and it consists of a metal, its oxide, and a small amount of carbonic elements. Agglomerates are formed on the surface of the SL and are then supplied to the gas phase. The formation of the SL is related to the propellant structure, which can be determined via the ratio between the ignition temperature of the MF particles and the decomposition temperature of the carbon skeleton. In the present work, a large amount of burning particles is observed in all six propellants. The oxide in the SL is in liquid form (Figs. 8 and 9), and 'inter-pocket' agglomeration is observed at a relatively low pressure of 0.5 MPa. These observations suggest that the SL mode belongs to 'type A' [32], with metal combustion occurring within the SL in the presence of a high degree of binding of the metal particles with the SL elements.

Although our laser ignition tests show that all the alloys tested here can promote Al ignition, only Al-Ni and Al-Mg can reduce the agglomerate size. This suggests that the ignition of metallic fuel is not the main limiting factor in the agglomeration process. Instead, the adhesive force is critical to detachment because agglomerating particles can be considered to be droplets on a wettable surface [32]. Detachment of the agglomerates is controlled by a balance between aerodynamic forces (drag) and the sum of the adhesive forces and gravity, as illustrated in Fig. 11(b). In fact, the high percentage of metal and its oxide binding within the SL raises the possibility of the fusion of the original particles, with the presence of adhesion between growing particles and the SL elements providing for their retention on the burning surface and for further growth. The breaking-away of the particles from the SL surface occurs when the adhesive forces are weaker than the separation forces. According to Ref. [34], the presence of Ni alters the aluminum-oxide surface properties and weakens the adhesive forces. Faster detachment of the agglomerates from the burning surface can thus be expected, preferentially reducing the number of large particles. This is evidenced by examining the XRD patterns

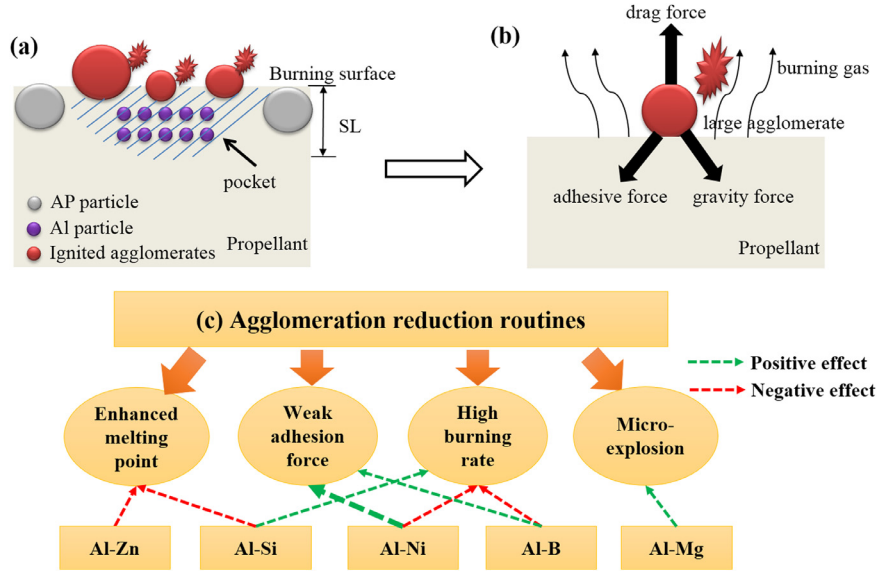

Fig. 11. Schematic of the proposed phenomenological agglomeration mechanism for propellants containing metallic-alloy particles: (a) agglomeration in the condensed layer, (b) agglomeration on the burning surface, and (c) agglomeration reduction mechanisms for five different alloy propellants, with the line thickness indicating the strength of the effect. (For interpretation of the references to colour in this figure legend, the reader is referred to the web version of this article.)

of the combustion products (see Fig. 10). The condensed combustion products of the baseline Al propellant is just Al_2O_3, but $Al_{2.66}O_4$ is found in the main products of almost all the alloy propellants. The presence of NiO in Al-Ni may weaken the adhesive forces between the agglomerates and the SL elements. The adhesive forces of Al-B are thought to be weakened by the low melting point of boron oxide, as the surface tension of metallic fuels typically decreases with the melting point. A weak adhesive force, therefore, counteracts the negative effect of a low burning rate in the Al-B propellant.

The pocket model of Cohen [1] has been widely used, despite it not capturing the underlying propellant structure in full [36]. According to this model, metal agglomeration is initiated from the melting of metal within a pocket in the inner condensed layer of the solid propellant. It is thought that the amount agglomerated is proportional to the amount of metal that melts within the pocket. Therefore, melting is another critical step towards agglomeration, with a high melting point being a hindrance to agglomeration. Figure 9(b) shows a significant molten layer on the burning surface of the Al-Zn propellant. The presence of large irregular agglomerates highlights the importance of melting-point effects in Al-Zn agglomeration.

Aside from adhesive forces and the melting point, the burning rate and particle micro-explosions are also important factors influencing agglomeration. When a large agglomerate is formed, it resides on the burning surface. The residence time is thus critical to determining the final size of the particles [19], with a shorter residence time leading to reduced agglomeration. For a given agglomerate, a higher burning rate is the third way in which agglomeration can be reduced, because it leads to a shorter residence time. The agglomerate size of the Al-Si propellant highlights the importance of the burning rate. As for Al-Mg, we find that this metallic alloy mainly alters the agglomerate size via particle micro-explosions in the propellant plume. Although the oxide of the Al-Mg propellant, i.e. $Mg_{0.388}Al_{2.408}O_4$, can change the attribution of adhesive forces, particle micro-explosions are still believed to be the dominant factor [7].

From the analysis presented above, we can develop a phenomenological mechanism for agglomeration in metallic-alloy propellants. As illustrated in Fig. 11, weak adhesive forces between an oxide and the SL elements, a high burning rate, and micro-explosion events are thought to inhibit agglomeration, while a low melting point is thought to enhance agglomeration. These four effects are believed to dominate the agglomeration process, but not all of them are equally active in all metallic-alloy propellants. For example, Al-Ni has roughly the same melting point as the baseline Al, but it shows less agglomeration because the positive effect of a weak adhesive force dominates the negative effect of a low burning rate. A low melting point dominates agglomeration in Al-Zn, ultimately resulting in larger agglomerates. The competing effects for Al-Si are a low melting point and a high burning rate, whereas agglomeration in Al-B is determined by a weak adhesive force and a low burning rate, leading to a similar agglomerate size for these two different propellants. It should be noted that Al-Mg alters agglomeration via particle micro-explosions in the propellant plume.

4. Conclusions

In this experimental study, we have investigated the substitution of aluminum particles with metallic alloys so as to reduce agglomeration in solid composite propellants. We considered five different aluminum-based alloys: Al-Zn, Al-Si, Al-Ni, Al-Mg and Al-B. Through TG-DSC measurements, we found that all five alloys can promote oxidation and ignition relative to the baseline Al particles, although only Al-Si and Al-Zn had lower melting points. Through laser ignition experiments, we found that Al-Mg exhibits the most balanced combination of a short ignition delay time and a short self-sustaining combustion time. At pressures between 0.5 and 3 MPa, we found that Al-Si had the highest burning rate, while Al-Ni and Al-Mg had the lowest pressure exponents. High-speed microscopic surface imaging at 0.5 and 1 MPa showed that Al-Ni produced the least agglomeration, but that Al-Zn produced the most, with Al-Si performing similarly to the baseline Al propellant. We then proposed a qualitative phenomenological mechanism for agglomeration based on a competition among four distinct effects: the metal melting temperature, the adhesive force of the agglomerates, the propellant burning rate, and micro-explosions. It is speculated that agglomeration can be reduced by deploying a metallic alloy with a weak adhesive force, a high burning rate, a high melting point, and particle micro-explosions. This would

open up new possibilities for the optimization of agglomeration and combustion characteristics using the metallic-alloy combinations studied here. Future work could focus on the development of new two-component alloys, or even three-component alloys, to achieve more effective agglomeration suppression based on the criteria considered in this study.

Declaration of Competing Interest

None.

Acknowledgments

This work was funded by the Natural Science Basic Research Plan in Shaanxi Province, China (Grant No. 2018JQ5112), the Fundamental Research Funds for Central Universities (Grant No. 3102018ZY003), the Provincial College Students Innovation and Entrepreneurship Training Program (Grant No. S201910699388), and the Key Foundation of Equipment Development Department (Grant No. 6140720020101). The authors would like to thank Dr. Shixi Wu and Mrs Chongyang Zhou for providing the alloy powder and propellant samples.

References

[1] N.S. Cohen, A Pocket Model for Aluminum Agglomeration in Composite Propellants, AIAA J 21 (1983) 720–725.
[2] K. Nagendra, C. Vijay, P.A. Ramakrishna, Binder melt: quantification using SEM/EDS and its effects on composite solid propellant combustion, Proc. Combust. Inst. (2018).
[3] K. Gnanaprakash, S.R. Chakravarthy, Effect of binder melt flow on the leading edge flames of solid propellant sandwiches, Proc. Combust. Inst. (2018).
[4] T.R. Sippel, S.F. Son, L.J. Groven, S. Zhang, E.L. Dreizin, Exploring mechanisms for agglomerate reduction in composite solid propellants with polyethylene inclusion modified aluminum, Combust. Flame 162 (2015) 846–854.
[5] T.R. Sippel, S.F. Son, L.J. Groven, Aluminum agglomeration reduction in a composite propellant using tailored Al/PTFE particles, Combust. Flame 161 (2014) 311–321.
[6] D.S. Sundaram, V. Yang, Effects of entrainment and agglomeration of particles on combustion of nano-aluminum and water mixtures, Combust. Flame 161 (2014) 2215–2217.
[7] B. Hatem, H.C. W., G.I. E., O. Volkan, S.S. F., Ignition and combustion behavior of mechanically activated Al–Mg particles in composite solid propellants, Combust. Flame 194 (2018) 410–418.
[8] H. Wang, M. Rehwoldt, D.J. Kline, T. Wu, P. Wang, M.R. Zachariah, Comparison study of the ignition and combustion characteristics of directly-written Al/PVDF, Al/Viton and Al/THV composites, Combust. Flame 201 (2019) 181–186.
[9] A.G. Korotkikh, O.G. Glotov, V.A. Arkhipov, V.E. Zarko, A.B. Kiskin, Effect of iron and boron ultrafine powders on combustion of aluminized solid propellants, Combust. Flame 178 (2017) 195–204.
[10] H. Wei, L. Pei-Jin, G. Feiyan, T. Bowen, G. Jian, Y. Zhijian, Y. Qi-Long, Tuning the reactivity of metastable intermixed composite n-Al/PTFE by polydopamine interfacial control, ACS Appl. Mater. Interfaces 10 (2018) 32849–32858.
[11] W. Ao, P. Liu, H. Liu, S. Wu, B. Tao, X. Huang, L.K.B. Li, Tuning the agglomeration and combustion characteristics of aluminized propellants via a new functionalized fluoropolymer, Chem Eng J (2020) 382.
[12] D. Reese, L. Groven, S. Son, A. Mukasyan, Intermetallic compounds as fuels for composite rocket propellants, AIAA J (2013).
[13] S.K. Valluri, D. Bushiri, M. Schoenitz, E. Dreizin, Fuel-rich aluminum-nickel fluoride reactive composites, Combust. Flame 210 (2019) 439–453.
[14] B.C. Terry, M.A. Rubio, I.E. Gunduz, S.F. Son, Altering agglomeration in a composite propellant with aluminum-silicon eutectic alloy, J Propul Power (2019).
[15] B.C. Terry, I.E. Gunduz, M.A. Pfeil, T.R. Sippel, S.F. Son, A mechanism for shattering microexplosions and dispersive boiling phenomena in aluminum–lithium alloy based solid propellant, Proc. Combust. Inst. (2016), doi:10.1016/j.proci.2016.06.099.
[16] M.A. Xue, J.-H. Wu, S. Ye, D. Hu, X.-D. Yang, Y.-P. Wang, W.-J. Zhu, C.-B. Li, Shock-induced fast reactions of zinc nanoparticles and RDX, J. Phys. D Appl. Phys. 41 (2008) 045501.
[17] W. Wang, H. Zou, S. Cai, The oxidation and combustion properties of gas atomized aluminum−boron−europium alloy powders, Propellants, Explos., Pyrotech. (2019).
[18] W. Ao, X. Liu, H. Rezaiguia, H. Liu, Z. Wang, P. Liu, Aluminum agglomeration involving the second mergence of agglomerates on the solid propellants burning surface: experiments and modeling, Acta Astronaut 136 (2017) 219–229.
[19] X. Liu, W. Ao, H. Liu, P. Liu, Aluminum agglomeration on burning surface of NEPE propellants at 3–5MPa, Propell Explos Pyrot 42 (2017) 259–267.
[20] H. Liu, W. Ao, P. Liu, S. Hu, X. Lv, D. Gou, H. Wang, Experimental investigation on the condensed combustion products of aluminized GAP-based propellants, Aerosp Sci Technol (2020) 97.
[21] W. Yang, W. Ao, J. Zhou, J. Liu, K. Cen, Y. Wang, Impacts of Particle Size and Pressure on Reactivity of Boron Oxidation, J Propul Power 29 (2013) 1207–1213.
[22] Y.N. Zhou, J.Z. Liu, D.L. Liang, W. Shi, W.J. Yang, J.H. Zhou, Effect of particle size and oxygen content on ignition and combustion of aluminum particles, Chin. J. Aeronaut. 30 (2017) 1835–1843.
[23] S. Hasani, M. Panjepour, M. Shamanian, The Oxidation Mechanism of Pure Aluminum Powder Particles, Oxid Met 78 (2012) 179–195.
[24] W. Ao, J.H. Zhou, W.J. Yang, J.Z. Liu, Y. Wang, K.F. Cen, Ignition, combustion, and oxidation of mixtures of amorphous and crystalline boron powders, Combust Explo Shock+ 50 (2014) 664–669.
[25] R. Lomba, P. Laboureur, C. Dumand, C. Chauveau, F. Halter, Determination of aluminum-air burning velocities using PIV and Laser sheet tomography, Proc. Combust. Inst. (2018).
[26] M.J. Spalding, H. Krier, R.L. Burton, Boron suboxides measured during ignition and combustion of boron in shocked Ar/F/O2 and Ar/N2/O2 mixtures, Combust. Flame 120 (2000) 200–210.
[27] G. Schloeffel, A. Eichhorn, H. Albers, C. Mundt, F. Seiler, F. Zhang, The effect of a shock wave on the ignition behavior of aluminum particles in a shock tube, Combust. Flame 157 (2010) 446–454.
[28] J.E. Crump, J.L. Prentice, K.J. Kraeutle, Role of scanning electron microscope in study of solid propellant combustion: behavior of metal additives, Combust. Sci. Technol (1969) 205–223.
[29] N. Kubota, Role of additives in combustion waves and effect on stable combustion limit of double-base propellants, Propell Explos 3 (1978) 163–168.
[30] A. Ishihara, M.Q. Brewster, T.A. Sheridan, H. Krier, The influence of radiative heat feedback on burning rate in aluminized propellants, Combust. Flame 84 (1991) 141–153.
[31] P.E. Desjardin, J.D. Felske, M.D. Carrara, Mechanistic model for aluminum particle ignition and combustion in air, J Propul Power 21 (2005) 478–485.
[32] edited by V.A. Babuk, V.A. Vasilyev, V.V. Sviridov, Formation of Condensed Combustion Products at the Burning Surface of Solid Rocket Propellant, In: solid Propellant Chemistry, Combustion, and Motor Interior Ballistics, in: V. Yang, T.B. Brill, W.Z. Ren (Eds.), Progress in Astronautics and Aeronautics, 185, American Institute of Aeronautics and Astronautics, Reston, VA (2000), pp. 749–776. Chapter 2.21.
[33] J.K. Sambamurthi, E.W. Price, R.K. Sigman, Aluminum agglomeration in solid-propellant combustion, AIAA J 22 (1984) 1132–1138.
[34] V.A. Babuk, V.A. Vassiliev, V.V. Sviridov, Propellant formulation factors and metal agglomeration in combustion of aluminized solid rocket propellant, Combust Sci Technol 163 (2001) 261–289.
[35] S. Gallier, A Stochastic Pocket Model for Aluminum Agglomeration in Solid Propellants, Propell Explos Pyrot 34 (2009) 97–105.
[36] L. Xiao, W. Pang, Z. Qin, J. Li, X. Fu, X. Fan, Cluster analysis of Al agglomeration in solid propellant combustion, Combust. Flame 203 (2019) 386–396.